PFC/JA-92-17

# Theory of Electron Cyclotron Resonance Laser Accelerators

Chen, C.

Plasma Fusion Center
Massachusetts Institute of Technology
Cambridge, MA 02139

June 1992

Submitted to Physical Review A.

This work was supported by the U.S. Department of Energy High Energy Physics Division.

# Theory of Electron Cyclotron Resonance Laser Accelerators

Chiping Chen
Plasma Fusion Center
Massachusetts Institute of Technology
Cambridge, Massachusetts 02139

## ABSTRACT

The cyclotron resonance laser (CRL) accelerator is a novel concept of accelerating continuous charged-particle beams to moderately or highly relativistic energies. This paper discusses prospects and limitations of this concept. In particular, the nonlinear coupling of an intense traveling electromagnetic wave with an electron beam in a guide magnetic field is studied, and the effects of wave dispersion on particle acceleration are analyzed. For a tenuous beam, it is shown in a single-particle theory that the maximum energy gain and the maximum acceleration distance for the beam electrons in CRL accelerators with optimal magnetic taper exhibit power-law scaling on the degree of wave dispersion (measured by the parameter $\omega/ck_{\|} - 1$). The maximum energy gain is found to be independent of the wave amplitude, and the accelerating gradient is proportional to the wave amplitude. A self-consistent multiparticle model, which confirms the validity of the scaling laws, is used to study the characteristics of CRL accelerators in moderately high-current, microwave regimes. The parameter regimes of experimental interest are identified. The possibility of building continuous-wave (CW) CRL accelerators is discussed. Finally, the results of simulation modelling of a multi-megavolt, X-band, electron CRL accelerator are presented.

PACS number: 07.77.+p

## I. INTRODUCTION

There has been growing experimental interest recently in the cyclotron resonance laser (CRL) accelerator [1]-[11], an advanced accelerator concept of producing charged-particle beams at moderately or highly relativistic energies using an intense coherent electromagnetic wave and a guide magnetic field configuration. This novel accelerator has the following advantages over conventional radio-frequency (RF) accelerators: i) acceleration of continuous beams without microbunches, ii) use of oscillators, not necessarily amplifiers, as driver, iii) use of smooth-wall structures to avoid breakdown problems, and iv) high duty factor of acceleration. It is compact in comparison with electrostatic accelerators which are bulky but capable of accelerating continuous charged-particle beams. In addition to these intriguing features, there is a variety of potential applications of CRL accelerators. These include: i) production of high-average-power charged-particle beams for material and chemical research, such as beam welding and waste treatment, ii) X-ray generation, and iii) coherent millimeter wave generation, to mention a few examples. Proof-of-principle CRL accelerator experiments [3],[7],[10],[11] so far have had limited success and demonstrated the acceleration of electrons up to $\sim 0.5$ MeV in the microwave regime. Few theoretical studies [6]-[9] of the characteristics and limitations of CRL accelerators have been reported.

In this paper, the nonlinear interaction of a continuous electron beam with an intense traveling electromagnetic wave in the CRL accelerator is analyzed theoretically in the regime where the axial phase velocity is greater than or equal to the speed of light in vacuum. In particular, a single-particle Hamiltonian formalism is used for the analysis of particle dynamics in a tenuous beam regime (Sec. II). It is shown that the maximum energy gain and the maximum acceleration distance for the beam electrons in CRL accelerators with optimal magnetic taper exhibit power-law scaling on the degree of wave dispersion (measured by the parameter $\omega/ck_{\|}-1$). The maximum energy gain is found to

be independent of the wave amplitude, and the accelerating gradient is proportional to the wave amplitude. Based on scaling calculations and presently available intense lasers and microwave sources, microwave CRL accelerators are identified as a practical concept in either pulse or continuous-wave (CW) operation, while optical CRL accelerators require stringent conditions and therefore are so far of only theoretical interest. The preliminary results of this paper have been reported elsewhere [9].

Three-dimensional multiparticle simulations are performed in our studies of the self-consistent interaction of an intense coherent traveling electromagnetic wave with a tenuous or moderately high-current electron beam in a guide field configuration (Sec III). We refer this interaction as the *inverse* cyclotron autoresonance maser interaction, because the underlying equations of motion describing such an interaction are identical to those governing the cyclotron autoresonance maser (CARM) [12]-[16]. The scaling laws are verified. The results of design modelling of a multi-megavolt electron CRL accelerator powered by a high-power X-band microwave source are presented. Finally, the possibility of building multi-megavolt CW electron CRL accelerators is discussed.

## II. SINGLE-PARTICLE THEORY AND SCALING PROPERTIES

We first consider the motion of a tenuous relativistic beam of electrons in the field configuration (Fig. 1) consisting of an intense circularly polarized electromagnetic wave and an applied axisymmetric guide magnetic field (with $\nabla \cdot \vec{B}_0 = 0 = \nabla \times \vec{B}_0$)

$$\vec{B}_0(\vec{x}) = B_{0z}(z)\vec{e}_z - \frac{1}{2}\frac{dB_{0z}(z)}{dz}(x\vec{e}_x + y\vec{e}_y) \ , \tag{1}$$

where $B_{0z}(z)$ is a linear function of the acceleration distance $z > 0$. We will later generalize $B_{0z}(z)$ to be a continuous function of $z$ [see Eq. (9)]. The electric and magnetic fields for both the wave and the solenoid can be expressed in cgs units as

$$\vec{E}(\vec{x},t) = -\frac{1}{c}\frac{\partial}{\partial t}\vec{A}(\vec{x},t) \ , \tag{2}$$

$$B_0(\vec{x}) + \vec{B}(\vec{x},t) = \nabla \times \vec{A}(\vec{x},t) \ , \tag{3}$$

where the normalized vector potential for the wave and guide fields is defined by

$$\frac{e}{mc^2}\vec{A}(\vec{x},t) = \Big[ - \Big(\frac{yz}{2c}\Big)\frac{d\Omega_c(z)}{dz} \ + \ a\cos(k_{||}z - \omega t)\Big]\vec{e}_x$$

$$+ \ \Big[\frac{x}{c}\Omega_c(z) \ - \ \Big(\frac{xz}{2c}\Big)\frac{d\Omega_c(z)}{dz} \ - \ a\sin(k_{||}z - \omega t)\Big]\vec{e}_y \ . \tag{4}$$

In Eqs. (2)-(4), $-e$ and $m$ are the electron charge and rest mass, respectively, $c$ is the speed of light in vacuum, $\Omega_c(z) = eB_{0z}(z)/mc$ is the nonrelativistic cyclotron frequency associated with $B_{0z}(z)$, $k_{||}$ = const is the axial wave number, and $a = e|\vec{E}|/mc\omega$ = const is the normalized wave amplitude. Because the beam is tenuous, both the wave amplitude $a$ and the axial wave number $k_{||}$ are considered to be constant in this section.

### A. Hamilton Equations of Motion

When synchrotron radiation losses are negligibly small, (which is the case for $\gamma mc^2 <$ 1 TeV) [8], the equations of motion for an individual test electron can be derived from the Hamiltonian

$$H(\vec{x},\vec{P},t) = [(cP_x + eA_x)^2 + (cP_y + eA_y)^2 + c^2P_z^2 + m^2c^4]^{1/2} \ . \tag{5}$$

It is convenient to apply a time-dependent canonical transformation from the Cartesian canonical variables $(\vec{x},\vec{P})$ to the generalized guiding-center variables $(\phi, Y, z', P_\phi, P_Y, P_{z'})$ [9],

$$x = -P_Y/m\Omega_{c0} + (2P_\phi/m\Omega_{c0})^{1/2}\sin(\phi - k_{||}z + \omega t) \ ,$$

$$y = Y - (2P_\phi/m\Omega_{c0})^{1/2}\cos(\phi - k_{||}z + \omega t) \ ,$$

$$z = z' \ ,$$

$$P_x = (2m\Omega_{c0}P_\phi)^{1/2}\cos(\phi - k_{||}z + \omega t) \ , \tag{6}$$

$$P_y = P_Y \ ,$$

$$P_z = P_{z'} + k_{||} P_\phi \ ,$$

where $\Omega_{c0} = \Omega_c(0)$. This transformation can be obtained by successive applications of the generating functions

$$F_3(P_x, P_y; \alpha, Y) = (1/m\Omega_{c0})[P_x P_y - (P_x^2/2)\tan\alpha] - Y P_y \tag{7}$$

and

$$F_2(\alpha, z; P_\phi, P_{z'}, t) = (kz - \omega t + \alpha) P_\phi + z P_{z'} \ . \tag{8}$$

Assuming transverse guiding-center drifts be small such that $Y \cong 0 \cong P_Y/m\Omega_c$, it is readily shown that the Hamiltonian in the new variables is an approximate constant of motion and can be expressed in the form

$$H'(\phi, z', P_\phi, P_{z'}) = -\omega P_\phi + \gamma mc^2$$

$$= -\omega P_\phi + \{2mc^2\Omega_c(z')P_\phi + 2a[2m^3c^6\Omega_c(z')P_\phi]^{1/2}\cos\phi + c^2(P_{z'} + k_{||}P_\phi)^2 + (a^2+1)m_0^2c^4\}^{1/2}, \tag{9}$$

where $\gamma mc^2$ is the total electron energy. Because Eq. (1) can be generalized to represent arbitrary piecewise linear taper, the Hamiltonian in Eq. (9) provides a good approximation to the problem for a continuous tapering of the guide field.

It has been shown [9] that change in $P_\phi$ is proportional to negative change in the number of photons in the driving wave and the constancy of $H'$ corresponds to the conservation law of the total energy of the electron plus photon system. For a uniform guide field ($\partial\Omega_c/\partial z = 0$), the axial momentum $P_{z'}$ is also a constant of motion, corresponding to the conservation law of the total axial momentum. From $P_{z'} = kP_\phi - P_z = \text{const}$ and $H' = -\omega P_\phi + \gamma mc^2 = \text{const}$, it readily follows that

$$\gamma(1 - \beta_{ph}\beta_z) = \text{const} \ , \tag{10}$$

where $\beta_{ph} = \omega/ck_{||}$ and $\beta_z = v_z/c = (P_{z'} + k_{||}P_\phi)/\gamma mc$.

The Hamilton equations of motion for an individual electron are

$$\frac{d\phi}{dt} = \frac{1}{\gamma}\Big[-\gamma\omega + \Omega_c + \frac{k_\parallel}{m}(P_{z'} + k_\parallel P_\phi)\Big] + \frac{a}{\gamma}\Big(\frac{mc^2\Omega_c}{2P_\phi}\Big)^{1/2}\cos\phi \ , \tag{11}$$

$$\frac{dz'}{dt} = \frac{1}{\gamma m}(P_{z'} + k_\parallel P_\phi) \ , \tag{12}$$

$$\frac{dP_\phi}{dt} = \frac{mc^2}{\omega}\frac{d\gamma}{dt} = \frac{a}{\gamma}(2mc^2\Omega_c P_\phi)^{1/2}\sin\phi \ , \tag{13}$$

$$\frac{dP_{z'}}{dt} = -\frac{P_\phi}{\gamma}\Big[1 + a\Big(\frac{mc^2}{2\Omega_c P_\phi}\Big)^{1/2}\cos\phi\Big]\frac{d\Omega_c(z')}{dz'} \ . \tag{14}$$

The first term in Eq. (11) is proportional to the frequency mismatch (or detuning) $\Delta\omega = \omega - k_\parallel v_z - \Omega_c/\gamma$. At the cyclotron resonance

$$\omega = k_\parallel v_z + \frac{\Omega_c}{\gamma} = \frac{\Omega_c}{\gamma(1 - \beta_z/\beta_{ph})} \ , \tag{15}$$

the electrons with different initial phases are rapidly bunched around a synchronous phase of $\phi_s \cong \pi/2$ by the sinusoidal forcing term in Eq. (11), and then they act like a macroparticle if the resonance is sustained. It is this bunching effect that justifies the validity of the single-particle approximation to the multiparticle problem, (provided that the beam emittance and energy spread are small throughout the acceleration process).

### B. Unlimited Autoresonant Acceleration

For an ideal, non-dispersive wave field with $\beta_{ph} \equiv \omega/ck_\parallel = 1$ and a uniform magnetic field $\Omega_c(z) = \Omega_{c0}$, Eq. (10) becomes

$$\gamma(1 - \beta_z) = \text{const} \ , \tag{16}$$

which is responsible for the so-called autoresonant phenomenon [1],[2]. That is, the resonance condition (15) holds for the entire acceleration process as long as it is satisfied initially. Therefore, for the electrons with the synchronous phase $\phi = \phi_s = \pi/2$ at the autoresonance, $d\phi/dt = 0$, and Eq. (13) is the only relevant equation of motion.

Integrating Eq. (13) with $\phi = \pi/2$ and $\Omega_c(z) = \Omega_{c0}$, we find that the instantaneous synchronous energy $\gamma_s(t)mc^2$ is given by

$$[\gamma_s(t) + 2h][\gamma_s(t) - h]^{1/2} = a\left(\frac{9\Omega_{c0}}{2\omega}\right)^{1/2} \omega t + \text{ const} , \tag{17}$$

where $h = H'/mc^2 = \text{const}$. For sufficiently large $t$, this leads to the well-known asymptotic scaling relation [2]

$$\gamma(t) = \left(\frac{9a^2\Omega_{c0}}{2\omega}\right)^{1/3} (\omega t)^{2/3} , \tag{18}$$

resulting in unlimited acceleration as $t \to \infty$.

It can also be shown that the synchronous electron orbit $(\phi_s, \gamma_s)$ is asymptotically stable. Indeed, expanding Eqs. (11) and (13) with small $\delta\phi(t) = \phi(t) - \phi_s$ and $\delta\gamma(t) = \gamma(t) - \gamma_s(t)$ yields

$$\frac{d\delta\phi}{dt} = -K_1(t)\delta\phi \quad \text{and} \quad \frac{d\delta\gamma}{dt} = -K_2(t)\delta\gamma , \tag{19}$$

where $K_1(t) = (a/\gamma_s)(mc^2\Omega_{c0}/2P_{\phi s})^{1/2}$ and $K_2(t) = (K_1/\gamma_s mc^2)(\omega P_{\phi s} - H')$ are positive and decrease monotonically for sufficiently large $t$.

### C. Wave Dispersion Effects and Scaling Laws

In practise, however, the driving wave field is dispersive with $d\omega/dk \neq \text{const}$ and $\beta_{ph} \neq 1$. Consequently, the autoresonance condition (16) is violated and only limited acceleration can be achieved. This is illustrated in Fig. 2, where a typical constant-$H'$ phase plane $(\phi, P_\phi)$ is plotted. In Fig. 2 each contour has a constant value of $P_{z'}$. Point A corresponds to an electron initially at the resonance with $\phi = \phi_s = \pi/2$, $\gamma = 1.15$, and $v_\perp/v_z \cong 0.2$. This electron gains $\sim 0.5$ MeV as it reaches point B. Note that change in $\gamma$ is given by $\Delta\gamma = \beta_{ph}\Delta(k_\parallel P_\phi/mc)$.

The magnetic field can be varied in order to maintain the resonance between the wave and the particle and, therefore, the acceleration process. By analyzing the Hamiltonian dynamics of the electron in various tapered guide field profiles, we find that the maximum

electron energy gain can be obtained by choosing an optimal taper such that $\phi(t) \approx \phi_s = \pi/2$ for the entire acceleration process. Figure 3 shows typical results of such an analysis. In Fig. 3, the electron kinetic energy and optimal axial magnetic field are plotted as a function of acceleration distance, for the choice of $a = 0.05$, $\beta_{ph} = 1.001$, and the initial conditions: $z = 0$, $\Omega_{c0}/ck_{||} = 0.595$, $\phi_0 = \pi/2$, $\gamma_i = 1.15$, and $v_{\perp 0}/v_{z0} = 0.2$ (initial pitch angle). The phase variation is within $\pm 8°$ for the normalized acceleration distance from $k_{||}z = 0$ to 500. It is evident that the degree of the taper has to become increasingly large in order to maintain the synchronous phase at the end of acceleration. Such an abrupt termination of acceleration allows us to estimate the values of the maximum acceleration distance $z_m$ and the maximum electron energy gain.

The maximum electron energy gain $G \equiv (\gamma_f - \gamma_i)/(\gamma_i - 1)$ and the maximum acceleration distance $k_{||}z_m$ are plotted in Fig. 4 for optimized systems. Both the gain and the distance exhibit a well-defined power-law dependence on the dispersion parameter $\beta_{ph} - 1$. The best fit of data yields the power-law scaling relations: $G \propto (\beta_{ph} - 1)^{-\mu}$ and $k_{||}z_m \propto (\beta_{ph} - 1)^{-\nu}$, with $\mu \cong 0.5$ and $\nu \cong 0.6$. For larger initial electron energies, both scaling relations hold as $\beta_{ph} \to 1$, but the value of energy gain decreases.

Although an analytical calculation of the values of the exponents $\mu$ and $\nu$ has not yet been available, the power-law scaling relations for the energy gain and acceleration distance are expected from the constant of motion defined in Eq. (10) and the resonance condition (15). Indeed, from Eqs. (10) and (15), the characteristic time scale for an initially resonant electron to dephase with respect to the wave is estimated to be $T \propto (\beta_{ph} - 1)^{-1}$, which we believe is responsible for the scaling behavior shown in Fig. 4.

The maximum energy gain is almost independent of the wave amplitude as shown in Fig. 5(a), where $G$ is plotted as a function of the normalized wave amplitude $a$. There is little change in the gain as $\beta_{ph} - 1$ varies by two orders of magnitude. Moreover, the axial magnetic field at the end of the acceleration is typically about twice its value at

$z = 0$, as shown in Fig. 5(b).

We conclude that CRL accelerators with optimal magnetic taper possess the following scaling properties

$$G \equiv \frac{\gamma_f - \gamma_i}{\gamma_i - 1} \propto \frac{1}{(\beta_{ph} - 1)^{0.5}} \quad \text{(independent of } a\text{)} \ , \tag{20}$$

$$k_{\|} z_m \propto \frac{1}{a(\beta_{ph} - 1)^{0.6}} \ , \tag{21}$$

$$\frac{B_{0z}(z_m)}{B_{0z}(0)} = 2 - 3 \ , \tag{22}$$

$$\text{accelerating gradient} \ \propto a \quad \text{(for a fixed } \beta_{ph}\text{)} \ . \tag{23}$$

From the above scaling laws, it is evident that an intense coherent radiation source with sufficiently large wave amplitude and sufficiently small dispersion $|\beta_{ph} - 1| \ll 1$ is a necessity in order to achieve high accelerating gradient and high energy gain.

In the microwave regime, the normalized wave amplitude on the $z$ axis and the dispersion parameter are given by

$$a = 1.7 \times 10^{-4} \left(\frac{[\text{cm}]}{r_w}\right) \left(\frac{[\text{GHz}]}{f}\right) \left(\frac{P}{[\text{W}]}\right)^{1/2} \ , \tag{24}$$

$$\beta_{ph} - 1 = 40 \times \left(\frac{[\text{cm}^2]}{r_w^2}\right) \left(\frac{[\text{GHz}^2]}{f^2}\right) \ , \tag{25}$$

respectively, Here, the condition $|\beta_{ph} - 1| \ll 1$ and the lowest-order transverse-electric cylindrical waveguide mode ($\text{TE}_{11}$) have been assumed, $f$ and $P$ are the frequency and power (or integrated axial Poynting flux) of the wave, respectively, and $r_w$ is the waveguide radius. For microwave electron CRL accelerators, high energy gain, $G = 10 - 100$, and moderately high accelerating gradient, 1-10 MeV/m, can be achieved with presently available high-power microwave sources, (assuming the initial electron kinetic energy $(\gamma_i - 1)mc^2 \sim 100$ keV). With a proper resonant cavity, a sizable wave amplitude ($a > 0.1$) can be achieved at a moderate input RF power level ($P \sim 1$ MW). This shows prospects for the production of high-average-power ($> 100$ kW), relativistic ($> 1$ MeV) electron

beams using continuous-wave (CW) CRL accelerators. Potential applications of high-average-power beams were mentioned in the Introduction.

In the optical regime, the normalized wave amplitude and the dispersion parameter are given by

$$a = 6 \times 10^{-6} \frac{\lambda}{[\mathrm{cm}]} \left( \frac{\text{Laser Intensity}}{[\mathrm{W/cm^2}]} \right)^{1/2} , \tag{26}$$

$$\beta_{ph} - 1 \approx \frac{\lambda^2}{2r_0^2} , \tag{27}$$

respectively. Here, $\lambda = 2\pi/k_{||}$ is the laser wavelength and $r_0$ is the characteristic laser beam radius. For example, a 1 $\mu$m, 10 $^{16}$ W/cm$^2$ Nd:glass-based laser yields a respectable wave amplitude, $a = 0.06$, and a small dispersion parameter, $\beta_{ph} - 1 \sim 10^{-8}$ (assuming $r_0 = 0.5$ cm). With presently available high-intensity lasers, accelerating gradient up to $\sim$ 100 MeV/m can be achieved [6]. However, the pulse length of such an ultra-intense laser is short, (typically of order 1 ps), which posses limitations on the optical CRL accelerator concept in practice. There are other problems as well, such as wave diffraction, slippage between the wave and the beam, and the requirement of a strong magnetic field.

## III. INVERSE CYCLOTRON AUTORESONANCE MASER

The scaling calculations in Sec. II.C have revealed that microwave CRL accelerators are most attractive from a practical point of view. The aim of this section is to develop a self-consistent theory of moderately high-current CRL accelerators in the microwave regime. In particular, the interaction of an electron beam and an intense microwave in the CRL accelerator is studied in a waveguide configuration using a three-dimensional, self-consistent, multiparticle model. We refer this interaction as an *inverse* cyclotron autoresonance maser interaction, because the underlying equations of motion describing such an interaction are identical to those describing the cyclotron autoresonance maser (CARM) [12]-[16]. The self-consistent evolution of the driving wave field and the beam

is studied.

### A. Self-Consistent CRL Accelerator Equations

In our model, a lossless cylindrical waveguide of radius $r_w$ whose axis coincides with the $z$-axis [or the axis of the axisymmetric guide field $\vec{B}_0(\vec{x})$] is assumed. The driving electromagnetic wave is expressed as a single-frequency transverse-electric (TE) waveguide mode, namely, the $TE_{11}$ mode. Because due to the inverse CARM interaction the amplitude and axial wave number of the wave varies slowly compared with the wave frequency, time averaging is performed over a wave period in order to obtain a set of slow-time-scale, self-consistent equations of motion describing the CRL accelerator. The effects of space-charge and transverse guiding-center drifts are ignored in the succeeding analysis.

Under the above assumptions, a complete set of self-consistent equations of motion governing the inverse CARM interaction has been derived and is expressed in the following dimensionless form [14],[15]

$$\frac{d\gamma}{d\hat{z}} = -2aX\left(\frac{\hat{p}_\perp}{\hat{p}_z}\right)\cos\psi \ , \tag{28}$$

$$\frac{d\hat{p}_z}{d\hat{z}} = -2aX\left(\frac{1}{\beta_{ph}} + \frac{d\delta}{d\hat{z}}\right)\left(\frac{\hat{p}_\perp}{\hat{p}_z}\right)\cos\psi - 2X\frac{da}{d\hat{z}}\left(\frac{\hat{p}_\perp}{\hat{p}_z}\right)\sin\psi - \frac{\hat{p}_\perp^2}{2\hat{p}_z B_{0z}}\frac{dB_{0z}}{d\hat{z}} \ , \tag{29}$$

$$\frac{d\psi}{d\hat{z}} = \frac{1}{\beta_{ph}} - \frac{\gamma}{\hat{p}_z} + \frac{d\delta}{d\hat{z}} + \frac{\hat{\Omega}_c}{\hat{p}_z} + \frac{2W}{\hat{p}_z\hat{p}_\perp}\left\{\left[\gamma - \hat{p}_z\left(\frac{1}{\beta_{ph}} + \frac{d\delta}{d\hat{z}}\right)\right]a\sin\psi + \hat{p}_z\frac{da}{d\hat{z}}\cos\psi\right\} \ , \tag{30}$$

$$\left(\frac{d^2}{d\hat{z}^2} + \beta_{ph}^{-2}\right)a(\hat{z})\exp\{i[\hat{z}/\beta_{ph} + \delta(\hat{z})]\} = \frac{ig}{\beta_{ph}}\left\langle X\left(\frac{\hat{p}_\perp}{\hat{p}_z}\right)\exp(i\psi)\right\rangle\exp\{i[\hat{z}/\beta_{ph} + \delta(\hat{z})]\} \ . \tag{31}$$

Equations (28)-(30) describe the dynamics of the beam electrons. In our simulations, we solve numerically $3N$ of such equations of motion for $N$ macroparticles representing the beam electrons, where $N = 1024$ is typical. The electron relative gyrophase is defined by

$$\psi = k_\parallel z + \delta(z) + \tan^{-1}(p_y/p_x) - \omega t - \pi/2 \ , \tag{32}$$

where $k_{\|} = (\omega^2/c^2 - k_\perp^2)^{1/2}$, $k_\perp = \nu/r_w$, and $\nu = 1.8418$ is the first zero of the derivative of the Bessel function of the first order $J_1'(x) = dJ_1(x)/dx$. Note that the relative gyrophase $\psi$ defined in the CARM literature differs from $\phi$ used in the single-particle analysis discussed in Sec. II. The normalized variables and parameters are defined by

$$\hat{p}_z = p_z/mc\ , \quad \hat{p}_\perp = p_\perp/mc\ , \quad \hat{z} = \omega z/c\ , \quad \beta_{ph} = \omega/ck_{\|}\ , \quad \hat{\Omega}_c = \Omega_c/\omega\ , \tag{33}$$

with $p_\perp = (p_x^2 + p_y^2)^{1/2}$. The geometric factors are

$$X(r_L, r_g) = J_1'(k_\perp r_L) J_0(k_\perp r_g)\ , \tag{34}$$

$$W(r_L, r_g) = \frac{J_1(k_\perp r_L)}{k_\perp r_L} J_0(k_\perp r_g)\ , \tag{35}$$

where the electron guiding-center radius $r_g$ is assumed to be an approximate constant of motion. Moreover, the $TE_{11}$ mode and the fundamental cyclotron frequency have been assumed. A general formalism that includes multiple waveguide modes and all harmonics of the cyclotron frequency has been presented elsewhere [14]-[15].

Equation (31) describes the self-consistent evolution of both the wave amplitude $a(z)$ and the axial wave number $k_{\|} + d\delta/dz$. In Eq. (31), the normalized coupling constant for the $TE_{11}$ mode is

$$g = \frac{4\beta_{ph}}{(\nu^2 - 1)J_1^2(\nu)} \left(\frac{ck_\perp}{\omega}\right)^2 \left(\frac{I_b}{I_A}\right)\ , \tag{36}$$

where $I_b$ is the beam current at the entrance of acceleration ($z = 0$) and $I_A = mc^3/e \cong 17$ kA is the Alfvén current. The notation $\langle F \rangle = N^{-1} \sum_{j=1}^{N} F_j$ denotes the ensemble average over the particle distribution.

The average RF power flow through the waveguide cross section at the acceleration distance $z$ is given by

$$P_w(z) = \frac{(\nu^2 - 1)J_1^2(\nu)}{2} \left(\frac{m^2c^5}{e^2}\right) \left(\beta_{ph}^{-1} + \frac{d\delta}{d\hat{z}}\right) \left(\frac{\omega}{ck_\perp}\right)^2 a^2\ . \tag{37}$$

The average beam power is

$$P_b(z) = (I_b/e)(\langle \gamma \rangle - 1)mc^2\ , \tag{38}$$

where the average electron mass factor is defined by

$$\langle\gamma\rangle = N^{-1}\sum_{j=1}^{N}\gamma_j(t_j,\tau_j(t_j,z))\ , \tag{39}$$

with $\tau_j(t_j,z) = t_j + \int_0^z dz/v_j$ being the time when the $j$th electron reaches the acceleration distance $z$. From Eqs. (28), (31), and (37)-(39), it is readily shown that the conservation law of energy, $P_b(z) + P_w(z) = \text{const}$, holds.

A three-dimensional simulation code that solves numerically the self-consistent CRL accelerator equations (28)-(31) has been developed for simulation studies of CRL accelerators in the microwave regime. It originates from our CARM amplifier code, CSPOT [14], which has been well benchmarked against kinetic theory in the linear regime and has shown good agreement with the CARM amplifier experiment [16]. The remainder of this paper discusses the results of our simulation studies.

### B. Verification of the Scaling Laws

Self-consistent multiparticle simulations of the wave-beam interaction in *tenuous* beam CRL accelerators have been performed extensively to verify the scaling properties obtained from the previous single-particle analysis. Because the beam is tenuous, both the wave amplitude and the axial wave number are almost constant.

Figure 6 shows logarithmic plots of the maximum electron kinetic energy gain $G \equiv (\langle\gamma_f\rangle - \langle\gamma_i\rangle)/(\langle\gamma_i\rangle - 1)$ and the maximum normalized acceleration distance $k_{\|}z_m$ as a function of the dispersion parameter $\beta_{ph} - 1$. In Fig. 6, the choice of system parameters corresponds to $a = 0.01$ in the single-particle analysis. The open squares are the results from the single-particle analysis shown in Fig. 4, and the solid circles are the results obtained from self-consistent multiparticle simulations using Eqs. (28)-(31). In the single-particle analysis, the initial conditions are $\gamma_i = 1.15$, $\phi_0 = \pi/2$, $v_{\perp 0}/v_{z0} = 0.05$, and $\omega = k_{\|}v_{z0} + \Omega_{c0}/\gamma_i$. In the self-consistent simulations, the initial conditions are the same as these in the single-particle analysis, except that the initial relative gyrophases of $N$

macroparticles $\psi_0$ are distributed uniformly from 0 to $2\pi$. The $TE_{11}$ mode of cylindrical waveguide is used and the RF frequency is $\omega/2\pi = 9.55$ GHz. The RF power is adjusted to yield a normalized wave amplitude of $a = 0.01$ on the $z$ axis as the waveguide radius (or $\beta_{ph}$) is varied. Waveguide effects result in somewhat longer acceleration distances than those from the one-dimensional single-particle analysis, because the effective wave amplitude is smaller off the axis. Moreover, a slight deviation from the synchronous gyrophase is allowed at the end of acceleration so that a larger gain in particle energy can be achieved. The gain enhancement is accompanied with undesirable increasing in energy spread. In any case, the best fit of data obtained from the self-consistent simulation confirms the scaling relations (20) and (21). Finally, the scaling relations (22) and (23) have also been confirmed for all parameter regimes investigated.

### C. Design Modelling of a Multi-Megavolt Electron CRL Accelerator

The scaling relations (20)-(23) and the self-consistent CRL accelerator equations (28)-(31) are readily applicable for design modelling of CRL accelerators. As an example, we discuss a moderately high-current, multi-megavolt electron CRL accelerator powered by a pulsed 20 MW, 11.4 GHz RF source (such as an X-band relativistic klystron amplifier). In this design study, the electron beam current is chosen to be sufficiently large so that the effects of changes in both the wave amplitude and the axial wave number due to the inverse CARM interaction can be examined. Figures 7 and 8 summarize the results of our design simulations which yield the electron energy gain $G = 30$, for the beam current $I_b = 2$ A and the initial beam voltage $V_i = 75$ kV. The effects of time-independent space-charge are not included in the simulation. The parameters in the simulation are given in Table I. For a $TE_{11}$ mode and the waveguide radius $r_w = 3.9$ cm, the normalized amplitude is $a = 0.017$ and the dispersion parameter is $\beta_{ph} - 1 = 0.02$, as evaluated from Eqs. (24) and (25). As discussed in Sec. II.C, use of a resonant cavity can reduce significantly the input RF power while maintaining the same or a larger wave amplitude.

The optimal axial magnetic field $B_{0z}$ and RF power are plotted in Fig. 7 as a function of the acceleration distance $z$. The axial magnetic field exhibits approximately a quadratic dependence on the distance $z$. It increases no more than three-fold throughout the entire accelerating distance. Significant RF power is converted into electron beam power, corresponding to 20% efficiency.

Figure 8 shows the phase space of the electrons, where the vertical axis is the electron kinetic energy and the horizontal axis is the electron gyrophase with respect to the phase of the RF field. In Fig. 8, only sixteen macroparticles are plotted at a given axial distance $z$. The initial energy (or axial momentum) spread is assumed to be negligibly small, and the final energy spread from the simulation is $\sigma_\gamma/\langle\gamma\rangle = 0.9\%$, where $\sigma_\gamma = (\langle\gamma^2\rangle - \langle\gamma\rangle^2)^{1/2}$.

## IV. CONCLUSIONS

The characteristics of electron cyclotron resonance laser (CRL) accelerators were analyzed theoretically. It was found that there exists a maximum energy threshold and a maximum acceleration distance. It was shown in a one-dimensional single-particle model that the maximum energy gain and the maximum acceleration distance obey certain scaling laws for optimized systems. The maximum energy gain is limited primarily by the degree of wave dispersion and is almost independent of the strength of the driving wave field. The validity of these scaling laws was confirmed in there-dimensional, self-consistent, multiparticle simulations in the microwave regime.

Based on our scaling calculations and presently available intense lasers and microwave sources, microwave CRL accelerators were identified as a practical concept in either pulse or continuous-wave (CW) operation, while optical CRL accelerators require stringent conditions and therefore are of only theoretical interest. A multi-megavolt, X-band, electron CRL accelerator experiment was proposed.

Although our analyses have focused primarily on a traveling-wave configuration, the

scaling laws are expected to be valid in a standing-wave configuration, a better representation of the driving wave in a resonant cavity. It is also straightforward to generalize the self-consistent CRL accelerator equations to the standing-wave configuration. Finally, we believe that the scaling laws and theory presented in this paper will provide important guidelines for future experimental studies of CRL accelerators.

## ACKNOWLEDGMENTS

The author wishes to thank G. Bekefi, B.G. Danly, R.J. Temkin, and J.S. Wurtele for helpful discussions. This work was supported by the U.S. Department of Energy High Energy Physics Division.

# References


[1] A.A. Kolomenskii and A.N. Lebedev, Soviet Physics, Dokl. **7**, 745 (1963).

[2] C.S. Roberts and S.J. Buchsbaum, Phys. Rev. **135**, 381 (1964).

[3] H.R. Jory and A.W. Trivelpiece, J. Appl. Phys. **39**, 3053 (1967).

[4] N.C. Luhmann, Jr. and A.W. Trivelpiece, Phys. Fluids **21**, 2038 (1978).

[5] K.S. Golovanevsky, IEEE Trans. Plasma Sci. **PS-10**, 120 (1982).

[6] P. Sprangle, L. Vlahos, and C.M. Tang, IEEE Trans. Nuclear Sci. **NS-30**, 3177 (1983).

[7] D.B. McDermott, D.S. Furuno, and N.C. Luhmann, Jr., J. Appl. Phys. **58**, 4501 (1985).

[8] A. Loeb and L. Friedland, Phys. Rev. **A33**, 1828 (1986).

[9] C. Chen, Phys. Fluids **B3**, 2933 (1991).

[10] R. Shpitalnik, C. Cohen, F. Dothan, and L. Friedland, J. Appl. Phys. **70**, 1101 (1991).

[11] R. Shpitalnik, J. Appl. Phys. **71**, 1583 (1992).

[12] V.L. Bratman, N.S. Ginsburg, G.S. Nusinovich, M.I. Petelin, and P.S. Strelkov, Int. J. Electron. **51**, 541 (1981).

[13] A.W. Fliflet, Int. J. Electron. **61**, 1049 (1986).

[14] C. Chen and J.S. Wurtele, Phys. Rev. Lett. **65**, 3389 (1990); Phys. Fluids **B3**, 2133 (1991).

[15] H.P. Freund and C. Chen, Int. J. Electron., in press (1992).

[16] A.C. DiRienzo, G. Bekefi, C. Chen, and J.S. Wurtele, Phys. Fluids **B3**, 1755 (1991).

Table I. Parameters for a Proposed 2.3 MeV CRL Accelerator

| Parameter | Symbol [Unit] | Value |
|---|---|---|
| Beam Current | $I_b$ [A] | 2 |
| Initial Beam Voltage | $V_i$ [kV] | 75 |
| Final Beam Voltage | $V_f$ [kV] | 2300 |
| Acceleration Distance | $z_m$ [cm] | 170 |
| Initial Axial Magnetic Field | $B_{0z}(0)$ [kG] | 2.43 |
| Final Axial Magnetic Field | $B_{0z}(z_m)$ [kG] | 7.0 |
| RF Frequency | $f$ [GHz] | 11.4 |
| RF Power | $P$ [MW] | 20 |
| Operating Mode | | $TE_{11}$ |
| Waveguide Radius | $r_w$ [cm] | 3.9 |

## FIGURE CAPTIONS

Fig. 1 Schematic of a CRL accelerator.

Fig. 2 Constant-$H'$ phase plane for $a = 0.05$, $\beta_{ph} = 1.001$, $H'/mc^2 = 1.079$, and $\Omega_{c0}/ck_{||} = 0.595$. Note that $\gamma = \beta_{ph}(k_{||}P_\phi/mc) - H'/mc^2$.

Fig. 3 The kinetic energy of an electron (solid curve) and optimal (normalized) axial magnetic field (dashed curve) as a function of the normalized acceleration distance $k_{||}z$, for $a = 0.05$, $\beta_{ph} = 1.001$, and the initial conditions $z = 0$, $\Omega_{c0}/ck_{||} = 0.595$, $\gamma_i = 1.15$, $\phi_0 = \pi/2$, and $v_{\perp 0}/v_{z0} = 0.2$.

Fig. 4 Shown in (a) the maximum kinetic energy gain and (b) the maximum normalized acceleration distance as a function of $\beta_{ph} - 1$, for $a = 0.01$, $v_{\perp 0}/v_{z0} = 0.05$, $\phi_0 = 0$, and $\gamma_i = 1.15$. The solid line is the best fit of data.

Fig. 5 (a) Maximum energy gain vs the normalized wave amplitude for $\beta_{ph} = 1.01$, $\phi_0 = \pi/2$, $\gamma_i = 1.15$, and $v_{\perp 0}/v_{z0} = 0.2$. (b) Ratio of final and initial axial magnetic fields vs the dispersion parameter $\beta_{ph} - 1$ for a = 0.05, $\phi_0 = \pi/2$, $\gamma_i = 1.15$, and $v_{\perp 0}/v_{z0} = 0.2$.

Fig. 6 Confirmation of the scaling relations (20) and (21).

Fig. 7 Axial magnetic field and RF power as a function of the acceleration distance for an X-band CRL accelerator.

Fig. 8 Phase space of beam electrons at several axial positions.

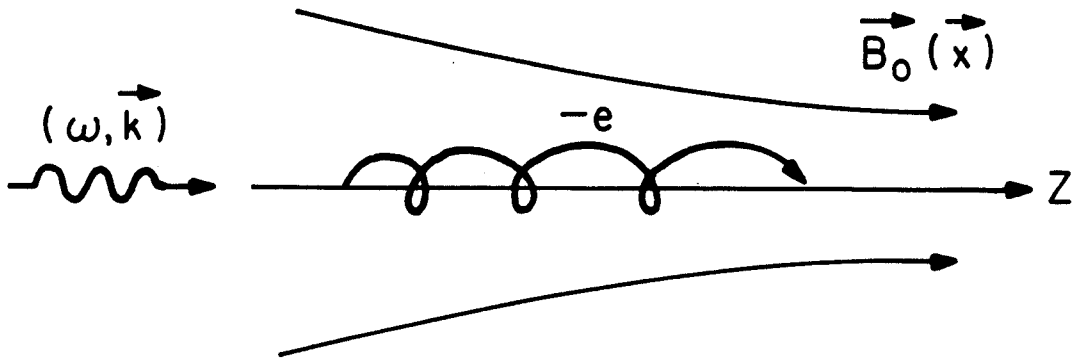


Fig. 1

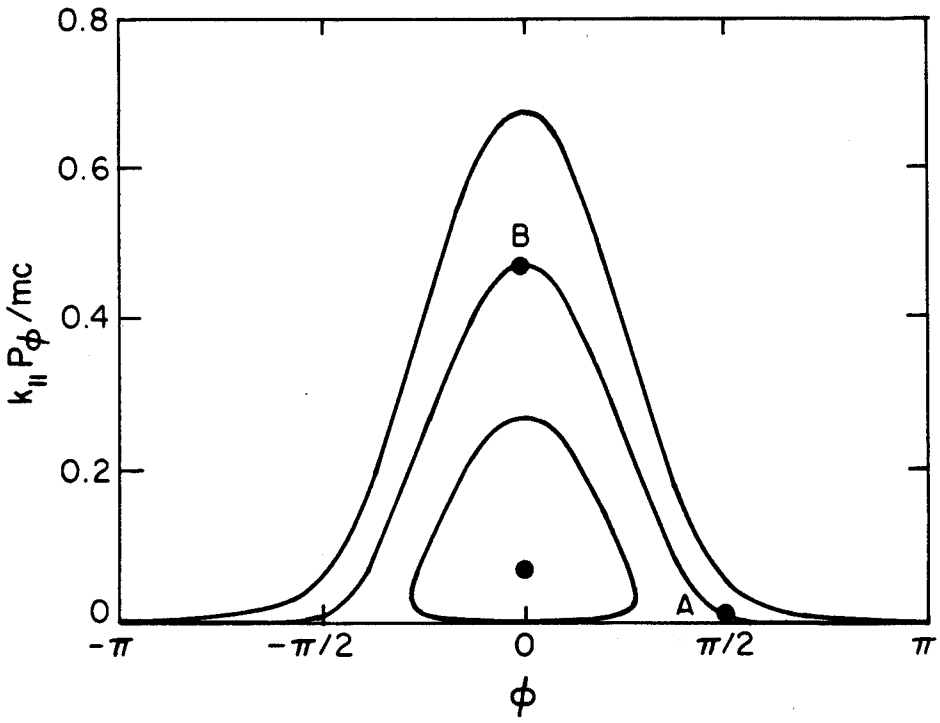


Fig. 2

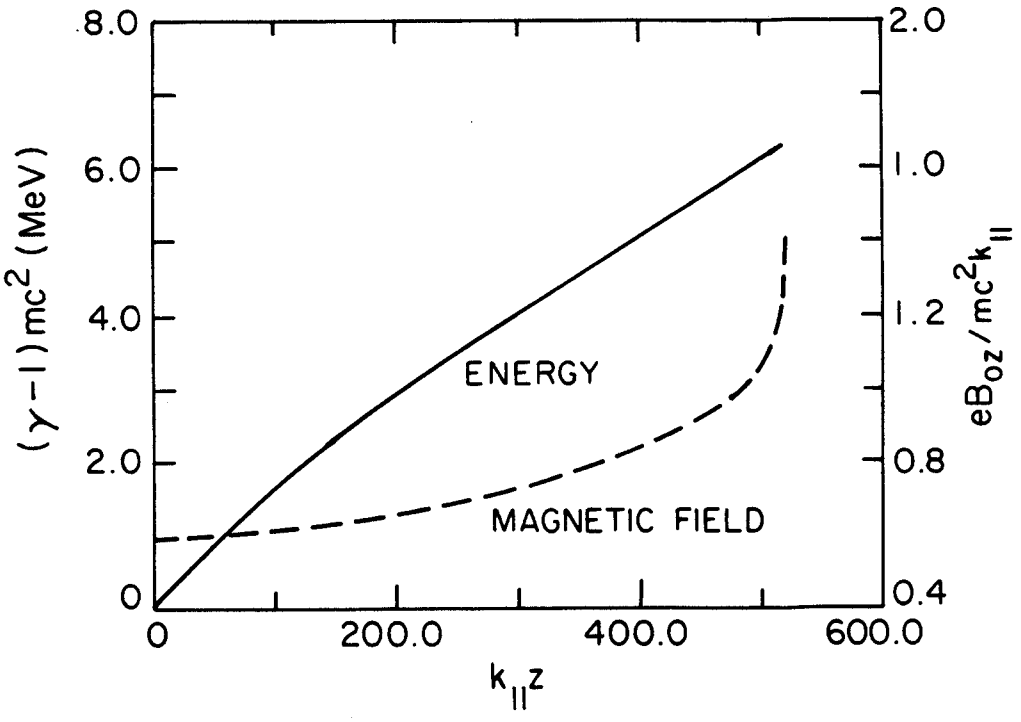
8.0
6.0
4.0
2.0
0
2.0
1.0
1.2
0.8
0.4
0
200.0
400.0
600.0
$(\gamma-1)mc^2$ (MeV)
$eB_{oz}/mc^2k_{\parallel}$
$k_{\parallel}z$
ENERGY
MAGNETIC FIELD

Fig. 3

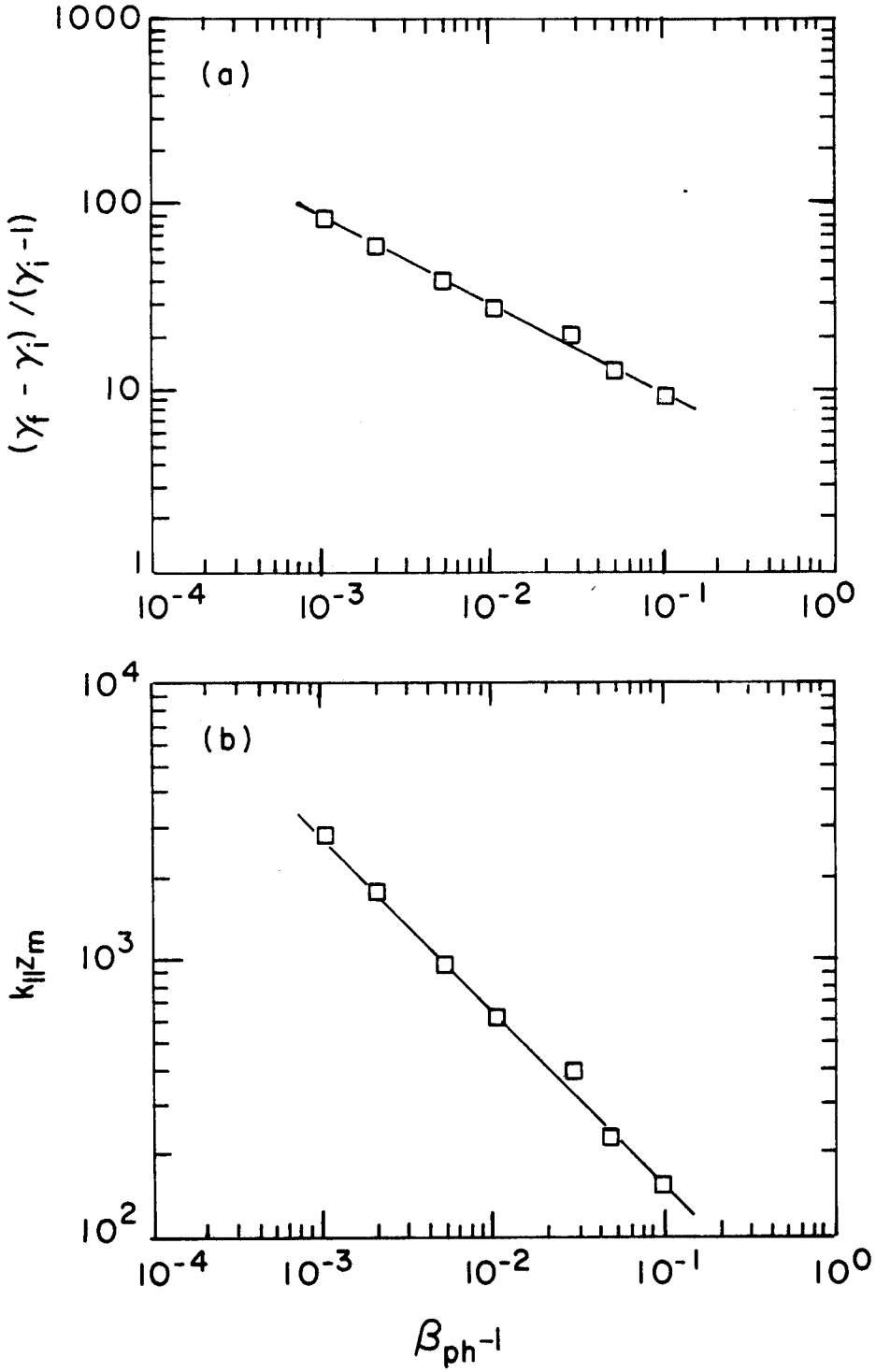
1000
100
10
1
(a)
$(\gamma_f - \gamma_i) / (\gamma_i - 1)$
$10^{-4}$
$10^{-3}$
$10^{-2}$
$10^{-1}$
$10^{0}$
$10^{4}$
$10^{3}$
$10^{2}$
(b)
$k_{\|} z_m$
$\beta_{ph}^{-1}$

Fig. 4

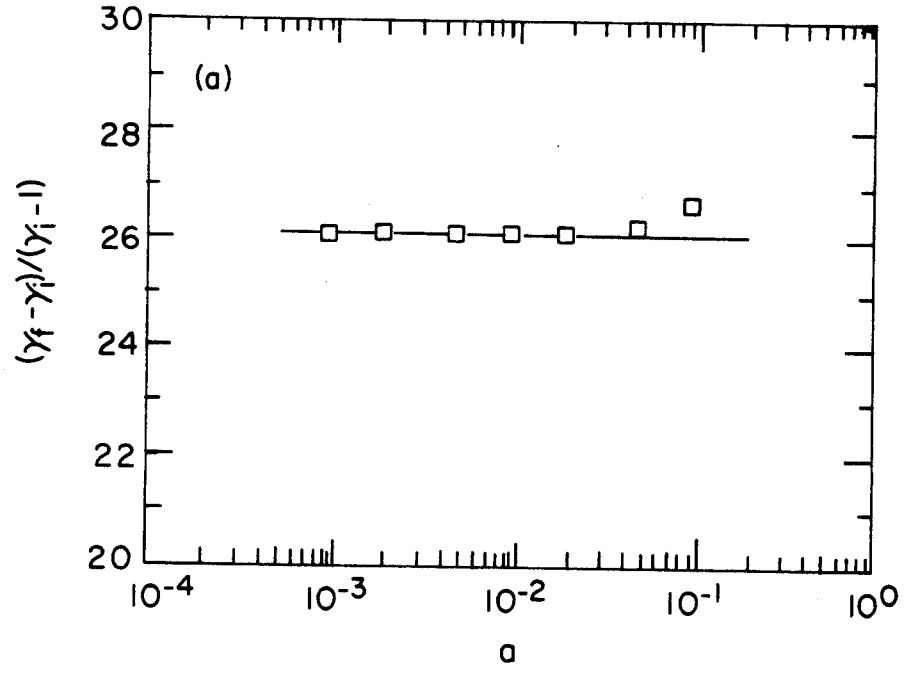
(a)
30
28
26
24
22
20
$(\gamma_f - \gamma_i)/(\gamma_i - 1)$
$10^{-4}$
$10^{-3}$
$10^{-2}$
$10^{-1}$
$10^{0}$
a

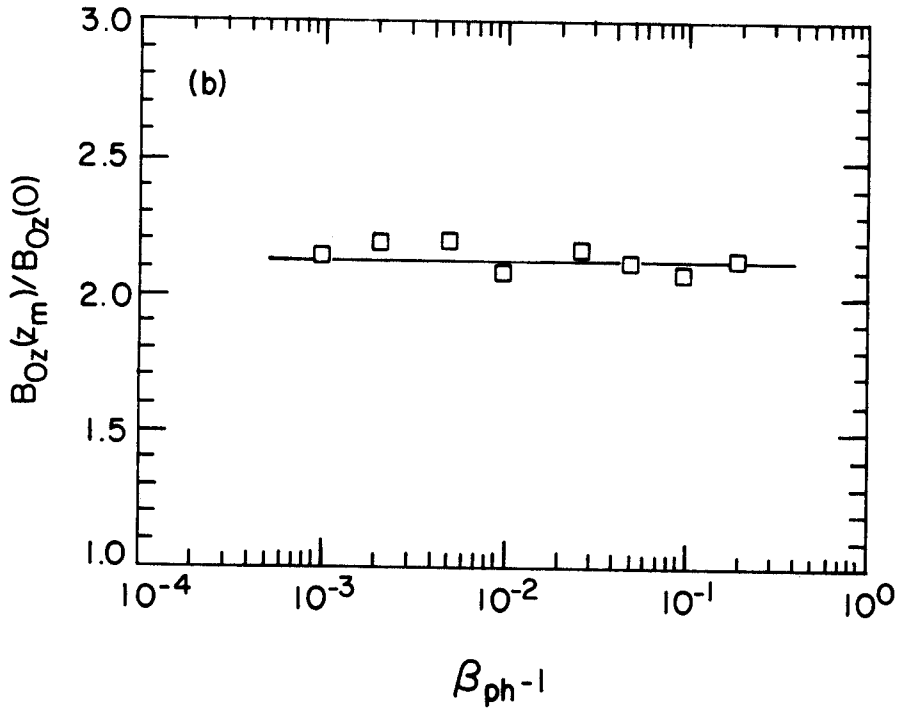
(b)
3.0
2.5
2.0
1.5
1.0
$B_{Oz}(z_m)/B_{Oz}(0)$
$10^{-4}$
$10^{-3}$
$10^{-2}$
$10^{-1}$
$10^{0}$
$\beta_{ph}-1$

Fig. 5

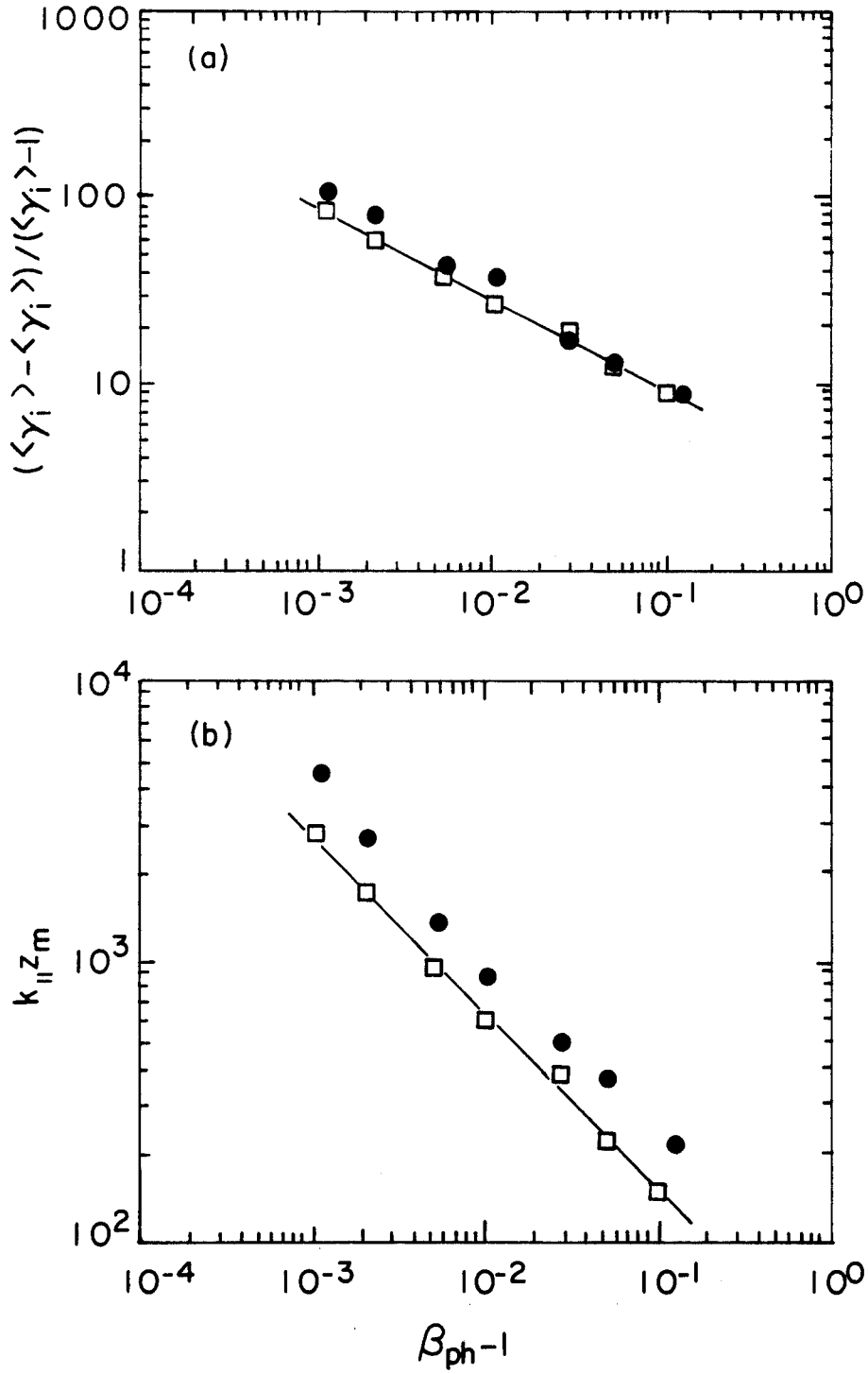
(a)
1000
100
10
1
$(\langle\gamma_i\rangle-\langle\gamma_i\rangle)/(\langle\gamma_i\rangle-1)$
$10^{-4}$
$10^{-3}$
$10^{-2}$
$10^{-1}$
$10^{0}$
(b)
$10^{4}$
$10^{3}$
$10^{2}$
$k_{\parallel} z_m$
$\beta_{ph}-1$

Fig. 6

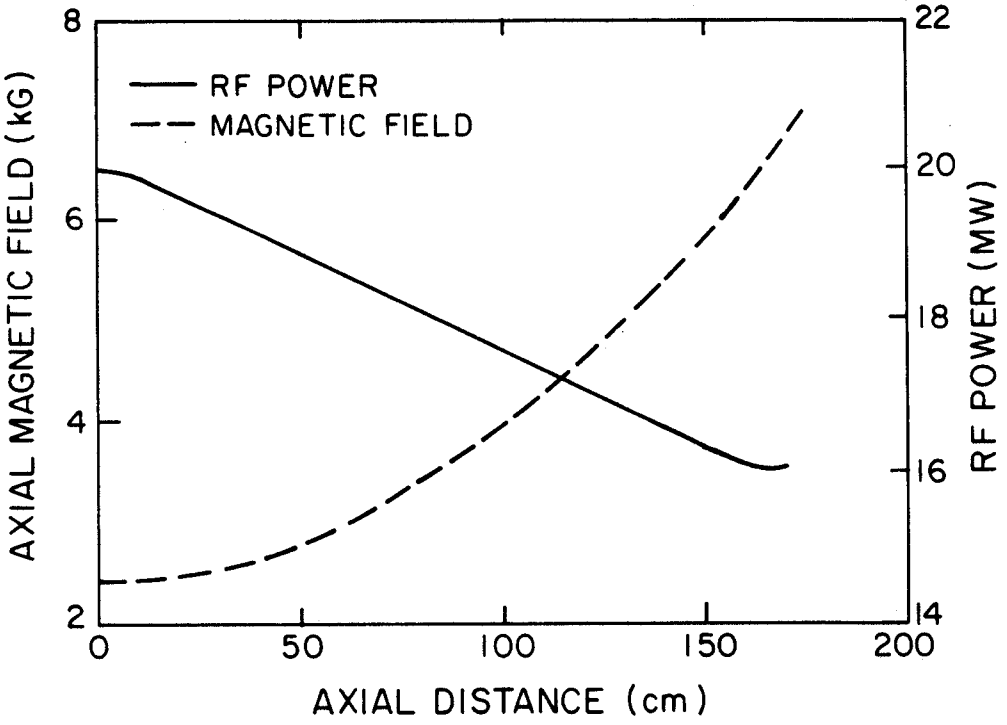
RF POWER
MAGNETIC FIELD
AXIAL MAGNETIC FIELD (kG)
RF POWER (MW)
AXIAL DISTANCE (cm)
8
6
4
2
22
20
18
16
14
0
50
100
150
200

Fig. 7

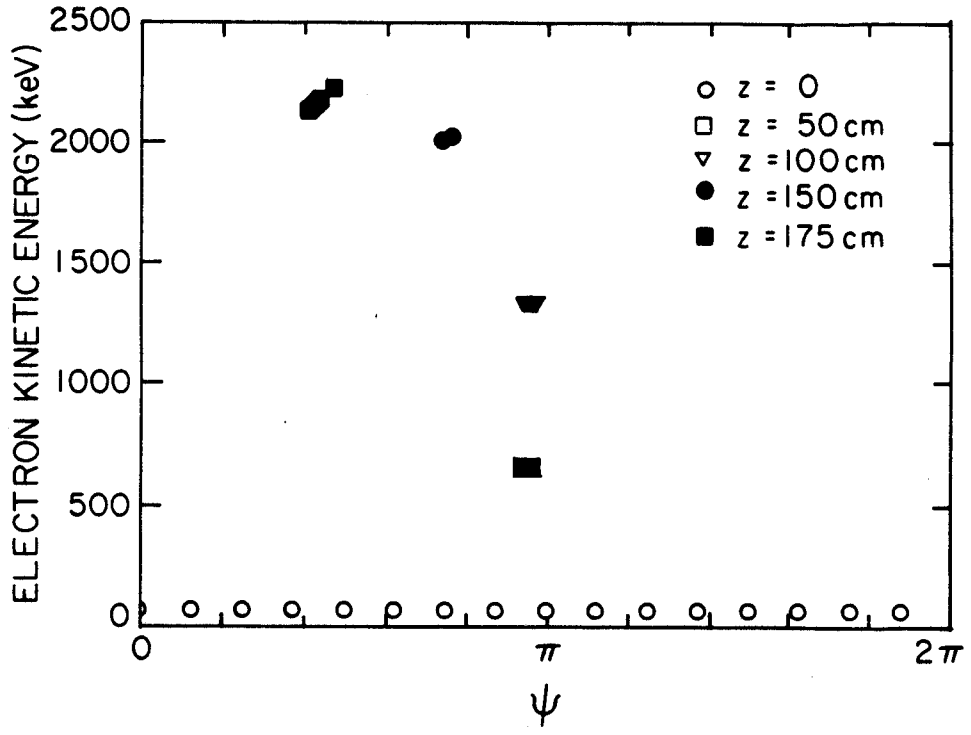
ELECTRON KINETIC ENERGY (keV)
2500
2000
1500
1000
500
0
0
π
2π
ψ
z = 0
z = 50cm
z =100cm
z =150cm
z =175cm

Fig. 8